ISSN 0018-151X, High Temperature, 2020, Vol. 58, No. 3, pp. 333–341. © Pleiades Publishing, Ltd., 2020.
Russian Text © The Author(s), 2020, published in Teplofizika Vysokikh Temperatur, 2020, Vol. 58, No. 3, pp. 355–364.

THERMOPHYSICAL PROPERTIES OF MATERIALS

Study of the Phase Boundary for C_6F_6 and SF_6 under Microgravity

V. S. Vorob'ev[a], E. E. Ustyuzhanin[b, *], V. F. Ochkov[b], V. V. Shishakov[b], Aung Tu Ra Tun[b], V. A. Rykov[c], and S. V. Rykov[c]

[a] *Joint Institute for High Temperatures, Russian Academy of Sciences, Moscow, 125412 Russia*
[b] *National Research University "Moscow Power Engineering Institute", Moscow, 111250 Russia*
[c] *University of Information Technologies, Mechanics and Optics (ITMO University), St. Petersburg, 197101 Russia*
**e-mail: evgust@gmail.com*

Received June 6, 2019; revised November 22, 2019; accepted December 24, 2019

Abstract—Two groups of experimental data obtained in the vicinity of the critical point are discussed. Group I describes the level h_l of the meniscus separating the two phases of the substance in the cell. The measurements were performed for SF_6 under the condition ($g = 9.8$ m s^{-2}) during an experiment conducted in a space laboratory. Group II includes data on the density of liquid and vapor measured for C_6F_6 along the saturation curve under terrestrial condition. In both cases, the studied two-phase sample is located in a horizontal cylindrical cell. In the second experiment, the gravitational effect was also measured along the isotherms as the dependence of the sample density on the height h measured from the bottom of the cell. An equation relating the h_l level (experiment I) with such functions as the order parameter f_s and the average diameter f_d is derived in this work. The obtained equation describes the initial experimental data at relative temperatures $\tau = (T - T_c)/T_c = 2 \times 10^{-6}$–0.01. An approach is considered that takes into account the influence under microgravity ($g = g_M \ll 9.8$ m s^{-2}) on the height h (experiment II). The dependences that represent f_s and f_d and the density of the liquid and gas phases along the saturation curve of these substances are obtained. These dependences agree satisfactorily with the results of experiments I and II in a wide temperature range and correspond to the scaling theory of critical phenomena.

DOI: 10.1134/S0018151X20030190

Introduction

The objects of this study are the (ρ_l, ρ_g, τ) data and functions $\rho_l(\tau)$, $\rho_g(\tau)$, $f_d(\tau)$, $f_s(\tau)$, etc., which are related to C_6F_6 and SF_6. Here, ρ_l and ρg are the densities of the liquid and gas phases, f_d is the average binodal diameter, f_s is the order parameter, $\tau = (T - T_c)/T_c$ is the relative temperature, and T_c is the critical temperature. The (ρ_l, ρ_g, τ) data for C_6F_6 were first measured in [1]. The density behavior along the SF_6 binodal was studied in several works [2–13], including experimental studies [9, 10]. The scaling models proposed in these publications are the functions $\rho_l(\tau)$, $\rho_g(\tau)$, $f_d(\tau)$, $f_s(\tau)$, etc., which correspond to the scaling theory (ST) of critical phenomena.

We can divide models $\rho_l(\tau)$ and $\rho_g(\tau)$ into two groups: one group generalizes the results [9], and the other is based on the data in [10]. The equations included in the first group and the same type equations of included in the second group differ; this difference applies to both the structure of the equations and the corresponding calculated data obtained with these functions. For example, in the region of relative temperatures of $\tau = 2 \times 10^{-4}$–0.01, we have

• a system of equations [6], which includes $f_d(\tau)$, $f_s(\tau)$ and contains linear and singular components; the average diameter $f_d(\tau) = B_{1-\alpha}\tau^{1-\alpha} + B_{2\beta}\tau^{2\beta} + B_1\tau + \ldots$, which is included in this system, was obtained from the data in [10]. Its structure contains five components, including scaling terms ($B_{2\beta}\tau^{2\beta}$, $B_{1-\alpha}\tau^{1-\alpha}$), which reflect the so-called "curvature" of this diameter (Fig. 1a, curve *2*); here, $B_{1-\alpha}$, $B_{2\beta}$, and B_1 are coefficients;

• a system of equations [4] containing only singular components and the diameter f_d, which corresponds to the eqaution $f_d(\tau) = B_{2\beta}\tau^{2\beta}$, obtained from the data in [10];

• diameter $f_d(\tau) = B_{1-\alpha}\tau^{1-\alpha} + B_1\tau$ [12], which includes two components obtained from the data in [10];

• diameter $f_d(\tau) = B_0 + B_1\tau$ [12] in the form of a rectilinear diameter, which is constructed from the (ρ_l, ρ_g, T) data related to the regular temperature range and measured in [10];

• functions corresponding to the linear form $f_d(\tau) =$ and recommended in [8, 9], the coefficients of which were found from the results of [9].

Concerning the known experimental (ρ_l, ρ_g, T) data, we concluded [2, 3] that the data of [9] and [10] noticeably differ. In [9], the (ρ_l, ρ_g, T) data were obtained by a direct method, i.e., in a piezometric experiment. At the first stage, the (ρ, P, T) data were

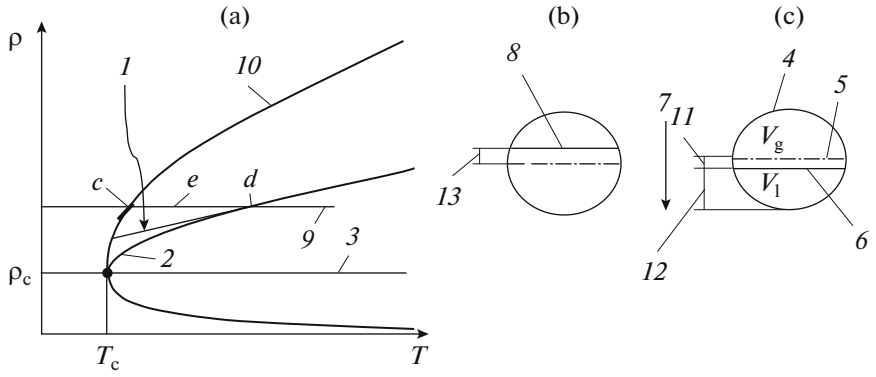

Fig. 1. (a) Binodal in the phase plane for SF_6: (*1*) the function $D_m = A_0 + A_1\tau$; (*2*) the function D_m constructed with the (ρ_l, ρ_g, T) data [10]; (*3*) isochore $\rho = \rho_{cell} = \rho_c$; (*9*) isochore $\rho = \rho_{cell} > \rho_c$; (*10*) bimodal; (b, c) cell and meniscus position in experiments II and I, respectively (*4*) a section of a cell having the shape of a horizontal cylinder; (*5*) virtual horizontal plane placed along the axis of the cylinder corresponding to the displacement h_{t0} and height h_{m0}; (*6*) the meniscus level at $\rho_{cell} < \rho_c$; (*7*) direction of gravity in the cell; (c) cell and position of the meniscus in experiment I: (*8*) the level of the meniscus at $\rho_{cell} > \rho_c$.

measured at the isotherm, where P is the pressure in the piezometer, e.g., in the liquid phase near the saturation curve. At the second stage, the ρ_l value was found via extrapolation of the (ρ, P) data to the boiling curve at $P = P_s$.

In [10], the (ρ_l, ρ_g, T) data were obtained indirectly, while direct measurements in the form of (ε_l, ε_g, T) data were used as initial data for the density. Here, ε_l and ε_g are dielectric constants measured by two sensors in the liquid and gas phases. The values of ε_l and ε_g substantially depend on the heights h_l and h_g of the dielectric-permittivity sensors in the cell. The vertical distances to the sensors h_l and h_g are measured from the bottom of the cell (as compared with the height h measured from the lower generatrix of the cylinder and determining the position of the density sensor in experiment II). No information is given in [10] on the values of h_l and h_g, the heights at which the two sensors recording the (ε_l, ε_g, T) data are located.

This inconsistency leads, on the one hand, to the fact that the dimensional mean diameter $D_m = (\rho_l + \rho_g)/2 = \rho_c(1 + f_d(\tau))$ (Fig. 1a, curve *2*) contains the function $f_d(\tau) = B_{1-\alpha}\tau^{1-\alpha} + B_{2\beta}\tau^{2\beta} + B_1\tau + \ldots$ [6], which is constructed with the (ρ_l, ρ_g, T) data [10]. Weiner first noted the curvature of this diameter in his dissertation in 1974[1]. Curve *2* substantially deviates from curve *1*, which represents the diameter $D_m = D_0 + D_1\tau$ [12].

On the other hand, the authors revealed additional information on the diameter $f_d(\tau)$ for SF_6. Garrabos et al. [8] carried out a special experiment I, which revealed that the gravitational effect is the cause of the curvature of diameter $f_d(\tau)$ in [10]. To confirm this conclusion, the cell used in experiment I [8], which has the shape of a horizontal cylinder (Fig. 1b) and contains a two-phase SF_6 sample, was placed under conditions (g = 9.8 m/s^2) in the space laboratory. Here, the meniscus displacement h_t was determined as the distance from the cylinder axis to the level of the meniscus separating the phases (Fig. 1b, line *8*). The data on h_t, T were measured along several near-critical isotherms. To generalize these data, the equation $h_t(\tau) = A(-B(f_d/f_s) + C/f_s)$ was proposed in [8]; it includes the functions f_d and f_s and the constants A, B, and C. The values of A, B, and C were determined from calibration experiments. In [8], several versions of the function $h_t(\tau)$ were considered, and several conclusions were drawn on the diameter $f_d(\tau)$:

- the diameter f_d significantly affects the function $h_t(\tau)$ and, therefore, the error contained in the model $f_d(\tau)$ determines to a large extent the error of $h_t(\tau)$;
- $h_t(\tau)$ (option A) includes the dependence $f_d(\tau)$ obtained in [6] based on the (ρ_l, ρ_g, T) data [10]. This option deviates significantly from the mentioned experimental (h_t, T) data. The measurements [10] and the dependence $f_d(\tau)$ [6] are associated with the gravitational effect; under microgravity conditions ($g = g_M$), the dependence $f_d(\tau)$ [6] is the reason that $h_t(\tau)$ (option A) is not consistent with the experimental (h_t, T) data [8];
- the linear dependence $f_d(\tau) = B_1\tau$ [8], which is based on the (ρ_l, ρ_g, T) data [9], is used in $h_t(\tau)$ (option B). This option decreases the deviation from the experimental (h_t, τ) data [8] in comparison with option A. This improvement indirectly indicates that the (ρ_l, ρ_g, T) data [10] contain an error that is a source of curvature (Fig. 1a, curve *2*) and significantly exceeds the error of the corresponding results [9].

For a detailed study of the role of gravity, the authors used the results of experiment II performed in

[1] Weiner, J., Breakdown of the law of rectilinear diameter, *Ph.D. Thesis*, Amherst: Univ. Massachusetts, 1974.

[1]. In the experiments [1], the authors obtained data on the gravitational effect, which takes place in a two-phase C_6F_6 sample placed in a cell made in the form of a horizontal cylinder (Fig. 1c). The gravitational effect is a dependence of $\rho(h)$, which includes the density ρ of the substance at fixed heights h counted from the lower generatrix of the cylinder (Fig. 1c, line *11*) at temperatures 515.98, 516.28, and 516.57 K (Figs. 2 and 3).

Experimental (ρ_l, ρ_g, T) data in the temperature range of 298.79–516.57 K and data on the saturation pressure P are also presented in [1]. Experiment II showed that the gravitational component of pressure ($P_g \approx \rho g h$), which is a component in the measured quantity P, leads to the following conclusion: the obvious distribution of $\rho(h)$, which under microgravity conditions ($g = g_M$) contains sections $\rho_l = \text{const}$, $\rho_g = \text{const}$ and the jump $\rho_l - \rho_g$ in the isotherm, turns into a continuous dependence of $\rho(h)$ (Figs. 2 and 3), while there is virtually no boundary in the sample as a meniscus between the liquid and gas phases located at a height h_m. The dependence $\rho(h)$, which refers to $T =$ 516.28 K (Fig. 3), includes an interval $2\Delta h$ ($\Delta h \approx \pm 2.2$ mm) near the axis of the cylinder, where the gravitational effect is significant.

The joint analysis of the results obtained in experiments I and II planned in this study makes it possible to estimate the quantitative effect of the gravitational component of P_g on the (ρ_l, ρ_g, T) data for C_6F_6 and SF_6. Experiment II showed that the gravitational effect significantly affects the function $\rho(h)$ as applied to C_6F_6 at constant external P, T. The deviation of the local density $\rho(h)$ at $\rho > \rho_c$ can differ from the corresponding density $\rho_l(T)$ by $\pm(2–10)\%$, depending on the height. These deviations indicate the level of errors that may be present in the (ρ_l, ρ_g, T) data [10] for SF_6.

The information presented for SF_6 (the variety of models, discrepancies in the experimental data on density, etc.) does not allow the user to give preference to the results of [9] over the results of [10] or to distinguish the equations included in the first group as more accurate in comparison with similar functions included in the second group. The construction of adequate models that describe a bimodal, diameter $f_d(\tau)$ and other functions for SF_6 in a critical region is an urgent problem.

In this work, we simultaneously assess the results obtained in experiments I and II, which are associated with the quantitative effect of the gravitational component of P_g on the (ρ_l, ρ_g, T) data for C_6F_6 and SF_6. The meniscus position is studied and, accordingly, the (ρ_l, ρ_g, T) data for C_6F_6 are corrected under the condition of a reduced gravitational effect in the cell [1]. The (ρ_l, ρ_g, T) data for SF_6 are calculated near T_c, which is not covered by the experiment, based on the experimental values of (h_t, T) [8].

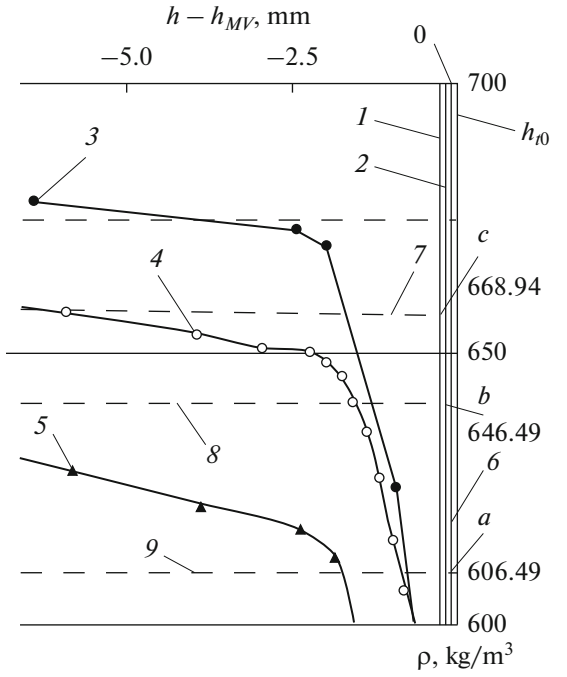

Fig. 2. Density distribution $\rho(h - h_m)$ for C_6F_6 along the isotherms in the region of high densities ($\rho > \rho_c$): (*a*–*c*) the intersection points of the isotherms $\rho_{mid}(h - h_m)$ with local meniscus levels (the calculated values of $\rho_l(T)$ are indicated); (*1*, *2*, *6*) values ($h - h_m$) corresponding to displacements h_t, (*3*, *4*, *5*) experimental (ρ, $h - h_m$) data, and (*7*, *8*, *9*) $\rho_{mid\,l}$ values at the temperatures of (*1*, *3*, *7*) 515.98, (*2*, *4*, *8*) 516.28, and (*6*, *5*, *9*) 516.57 K.

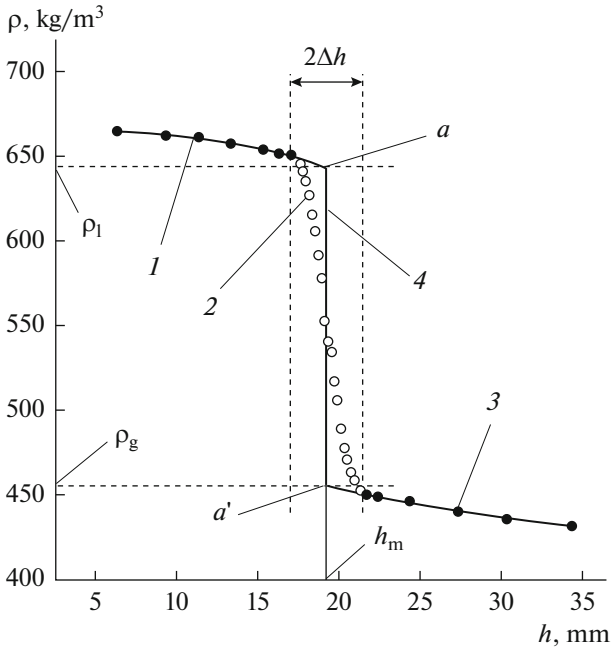

Fig. 3. Density distribution $\rho(h - h_m)$ for C_6F_6 at 516.28 K: (*a*, *a*') the intersection points of the approximating functions with the line $h = h_m$; (*1*) experimental (ρ, $h - h_m$) data for $\rho > \rho_c$; (*2*) experimental (ρ, $h - h_m$) data in the range of $2\Delta h$; (*3*) for $\rho < \rho_c$.

Table 1. Some results of the second stage of calculations for C_6F_6

ρ_l, kg/m^3	ρ_g, kg/m^3	τ	ρ_l, kg/m^3	ρ_g, kg/m^3	ur_{exp}	h_{texp}, mm	h_t, mm
670.3	433.7	0.00131	675.54	437.23	0.01268	0.191	0.207
644.8	455.8	0.000731	640.29	453.49	–0.00212	–0.031	0.157
610.1	491.5	0.000168	609.27	496.73	0.005059	0.079	0.078

We also found new expressions for the functions $\rho_l(\tau)$, $\rho_g(\tau)$, $f_d(\tau)$, etc. for C_6F_6 and SF_6 with a significant refinement of previously known results in the near-critical region.

MENISCUS POSITION IN THE CELL

In experiment II, the meniscus position in the cell is not estimated, but a method is proposed in which a virtual plane S_v is selected having height h_m (Fig. 3, line *4*). This height is $h_m = 19.1$ mm and is located in the vicinity of Δh near the cell axis (Figs. 2 and 3). The cell has a length of $L = 140.0$ mm and a diameter of $d = 40.0$ mm. In this method, experimental (ρ, h) the selected data were related, for example, to the isotherm $T = 516.28$ K (Fig. 3, curve *1*) at high densities ($\rho > \rho_c$), and were located outside Δh. Then, the (ρ, h) data were extrapolated to point *a* at the intersection with line *4* (Fig. 3). At this point, $\rho_l = 644.8$ kg/m^3 (Table 1). Similarly, we selected the experimental data (ρ, h) (Fig. 3, curve *3*) with low densities ($\rho < \rho_c$) that are located outside Δh. These (ρ, h) data were extrapolated to the point of intersection *a*' with line *4* (Fig. 3) to calculate the value of $\rho_g = 455.8$ kg/m^3 (Table 1).

It is of interest to determine the level h_{mT} at which the meniscus is placed in the cell (Fig. 1c). We selected the following boundary conditions:

• the average density of the sample $\rho_{cell} = M/V$ is determined by the equation $\rho_{cell} = \rho_c$; i.e., line *3* (Fig. 1a) is a critical isochore, and temperature T satisfies the inequality of $T < T_c$ (for example, $T = 516.28$ K);

• the gravitational effect is significantly decreased; the equilibrium density is $\rho_g(T)$ in the upper part of the cylinder and $\rho_l(T)$ is in the lower part; a meniscus forms in the cell due to the finite difference in densities ($\rho_l - \rho_g$).

The microgravity condition ($g = g_M$) can be created, for example, by mixing the substance in the upper part to a state that corresponds to the equilibrium value of ρ_g(T) and the same mixing of the substance in the lower part until the density $\rho_l(T)$ is reached.

To determine the meniscus level, we consider an isochoric process in a cell with a volume V (Fig. 1c). Let the substance in the initial state have parameters $\rho = \rho_c$, $T_1 = T_c$. We place the virtual horizontal plane S_v (Fig. 1c, line *5*) along the axis of the cylinder. This position is taken as the reference point h_{t0} (Fig. 2) for the displacement h_t (Fig. 1c, line *12*) of the meniscus that separates the two phases when the cell temperature decreases or rises. Let us select the upper and lower parts of the cell (V_g, V_l), which have a volume of $V/2$ (Fig. 1c).

We transfer the substance to state II. In this process, the following conditions are satisfied: $\rho_{cell} = \rho_c = \text{const}$, $T_{II} = T_c + \Delta T$. Here, ρ_{cell} is the average density of the substance in the cell, and $\Delta T > 0$. The substance becomes overheated in the cell with respect to the critical temperature, and the meniscus does not occur.

Next, we transfer the substance to state I. In this process, the following conditions are fulfilled: microgravity is reached ($g = g_M$), $\rho_{cell} = \rho_c = \text{const}$, $T_2 = \Delta T$, and $\Delta T > 0$. This results in

• condensation in the cell, which causes a decrease in the mass of the substance in the upper part ($\Delta M > 0$),

• a difference in the density of the gas phase ρ_g and the density of the liquid phase ρ_l; a meniscus forms due to microgravity and the finite difference ($\rho_l - \rho_g$), located below the cell axis and separating the two phases;

• a shift of the S_v plane down to the meniscus (Fig. 1c, line *6*); this displacement h_t is marked by line *12* (Fig. 1c).

The phase densities can be written as (ρ_g, ρ_l) = ($\rho_c + \Delta\rho_g\rho_c$, $\rho_c + \Delta\rho_l\rho_c$), where $\Delta\rho_l = (\rho_l - \rho_c)/\rho_c$, $\Delta\rho_g = (\rho_g - \rho_c)/\rho_c$. We write the volume V of the sample as a function of a number of arguments, including (ΔM, $\Delta\rho_g$, $\Delta\rho_l$), as

$$V = \left(\frac{M}{2} - \Delta M\right)\frac{1}{\rho_c + \Delta\rho_g\rho_c} + \left(\frac{M}{2} + \Delta M\right)\frac{1}{\rho_c + \Delta\rho_l\rho_c}. \quad (1)$$

The function $\Delta M/M$ is expressed from Eq. (1) as

$$\frac{\Delta M}{M} = \left(\frac{\Delta\rho_l + \Delta\rho_g}{2} + \Delta\rho_l\Delta\rho_g\right)\frac{1}{\Delta\rho_g - \Delta\rho_l}. \quad (2)$$

The functions f_d and f_s are introduced as

$$f_d = (\rho_l + \rho_g)(2\rho_c)^{-1} - 1 = (\Delta\rho_l + \Delta\rho_g)/2, \quad (3)$$

$$f_s = (\rho_l - \rho_g)(2\rho_c)^{-1} = (\Delta\rho_l - \Delta\rho_g)/2. \quad (4)$$

After some transformations, substituting Eqs. (3) and (4) into Eq. (2) with allowance for the equations $\Delta\rho_g - \Delta\rho_l = -2f_s$ and $\Delta\rho_g\Delta\rho_l = f_d^2 - f_s^2$, gives

$$\frac{\Delta M}{M} = \frac{f_s}{2} - \frac{f_d}{2f_s} - \frac{f_d^2}{2f_s}. \quad (5)$$

The change in the volume of the upper part is represented as

$$\Delta V_g = \left(\frac{M}{2} - \Delta M\right)\frac{1}{\rho_g} - \frac{V}{2}. \quad (6)$$

With Eqs. (5) and (6), the relative change in volume $\Delta V_g/V$ after transformations is written as

$$\frac{\Delta V_g}{V} = \left(\frac{\rho_c}{2} - \frac{\Delta M}{M}\rho_c\right)\frac{1}{\rho_c(1+\Delta\rho_g)} - \frac{1}{2} \simeq \left(\frac{1}{2} - \frac{\Delta M}{M}\right)(1-\Delta\rho_g) - \frac{1}{2}. \quad (7)$$

With the equation $\Delta\rho_g = f_d - f_s$ and Eqs. (5) and (7), the function $\frac{\Delta V_g}{V}$ can be written as follows:

$$\frac{\Delta V_g}{V} = \frac{(f_d + f_d^2 - f_s^2)(1+f_s+f_d)}{2f_s} - \frac{f_d - f_s}{2} = \frac{f_d}{f_s}\left(\frac{1}{2} + \frac{f_d f_s}{2} + \frac{f_d f_s^2}{2} + \ldots\right). \quad (8)$$

Let us consider the following conditions: $f_s > 0$ [7] and $\Delta V_g/V > 0$; i.e., the relative volume of the upper part increases in the isochoric process. Then, we can obtain the following inequality in the asymptotic temperature region ($\Delta T > 0$ is small) from Eq. (8):

$$f_d \approx \frac{2\Delta V_g}{V} f_s > 0. \quad (9)$$

Equation (9) is derived for the first time and is valid for any form of the functions $f_d(\tau)$, $f_s(\tau)$ under the specified conditions. We represent ΔV_g as an elementary sample volume and write the ratio $\Delta V_g/V$ as an approximate function with argument h_t, i.e.,

$$\frac{\Delta V_g}{V} = \frac{h_t L d}{L\frac{\pi d^2}{4}}. \quad (10)$$

The displacement h_t can be represented with Eqs. (8) and (10) in the form

$$h_t = \frac{\pi d}{8} ur, \quad (11)$$

where $ur = f_d/f_s$ is a temperature-dependent complex.

Equation (11) yields that the displacement h_t is not the only value that would correspond to the height ($h_m = 19.1$ mm) proposed in [1].

EVALUATION OF THE MENISCUS POSITION IN EXPERIMENT II AND SOME NUMERICAL DATA ON THE DENSITY OF C_6F_6

We propose the following approach to construct the function $h_t(T)$ as applied to the temperature conditions implemented in experiment II [1]. First, the combined models $f_s(C, D, \tau)$, $f_d(C, D, \tau)$ are selected to represent f_s, f_d in the form [2, 3, 13]

$$f_s = B_{s0}\tau^\beta + B_{s1}\tau^{\beta+\Delta} + B_{s2}\tau^{\beta+2\Delta} + B_{s3}\tau^2 + B_{s4}\tau^3, \quad (12)$$

$$f_d = B_{d0}\tau^{1-\alpha} + B_{d\exp}\tau^{2\beta} + B_{d1}\tau^{1-\alpha+\Delta} + B_{d3}\tau^2 + B_{d4}\tau^3, \quad (13)$$

where $D = (T_c, \rho_c, \alpha, \beta, \ldots)$ are the critical characteristics of the model, and $C = (B_{si}, B_{di})$ are coefficients.

First, we emphasize that there are no scaling models in the literature that describe the functions f_s, f_d, etc. in the critical region for C_6F_6. The values of C and D for Eqs. (12) and (13) were determined with the nonlinear least-squares method (NRMS) [5, 13] and experimental (ρ_l, ρ_g, T) data for C_6F_6 [1]. Second, the structure of models (12), (13) contains the leading scaling components $B_{d0}\tau^{1-\alpha}$, $B_{d0}\tau^{2\beta}$, which reflect current trends in the scaling theory [2, 3, 6, 13].

In the NRMS method, the following information is selected at the first stage:

- the initial approximation for D is as follows: $T_c = 516.62$ K [1], $\rho_c = 550.9$ kg/m^3 [1], $\alpha = 0.11$ [7], $\beta = 0.325$ [7], $B_{s0} = 2.0$ [7], $B_{d0} = 0.5$ [7], and $B_{d\exp} = 0.2$;
- the leading component f_d (Eq. (13)) corresponds to the inequality $B_{d\exp} > 0$ (see condition (9)).

At the second stage, the values of C and D are calculated: $T_c = 516.65$ K, $\rho_c = 550.43$ kg/m^3, $\alpha = 0.131$, $\beta = 0.348$, $B_{s0} = 2.145$, $B_{d0} = 0.595$, and $B_{d\exp} = 0.1005$.

The obtained models (12) and (13) served as the basis for the functions $\rho_l(\tau, D, C)$ and $\rho_g(\tau, D, C)$ in the following form:

$$\rho_l = (f_d + f_s + 1)\rho_c, \quad \rho_g = (f_d - f_s + 1)\rho_c. \quad (14)$$

Based on Eqs. (11)–(14), we obtained some numerical values. The (ρ_g, ρ_l, T) data were calculated along the isotherms [1]. The results are consistent with the (ρ_l, ρ_g, T) data [1] with acceptable accuracy in the range of $2 \times 10^{-4} < \tau < 0.2$. The root-mean-square (RMS) deviations of S_g, S_l for the (ρ_l, ρ_g, T) data [1] for the results of Eqs. (14) were $S_g = 0.52\%$ and $S_l = 0.12\%$.

The NRMS approach [5, 13] made it possible to determine the coefficients for the scaling part $f_{s\,\mathrm{scale}} = B_{s0}\tau^\beta + B_{s1}\tau^{\beta+\Delta} + B_{s2}\tau^{\beta+2\Delta}$, $f_{d\,\mathrm{scale}} = B_{d0}\tau^{1-\alpha} + B_{d\exp}\tau^{2\beta} + B_{d1}\tau^{1-\alpha+\Delta}$, which are included in Eqs. (12) and (13). The corresponding functions $\rho_l(\tau, D)$, $\rho_g(\tau, D)$ give satisfactory agreement with the experiment [1] in the range of $2 \times 10^{-4} < \tau < 0.1$, while the standard deviations are $S_g = 0.31\%$ and $S_l = 0.16\%$.

Table 1 presents some numerical results. The experimental density values and data on $ur_{\exp}$, $h_{t\,\exp}$, and T are also listed there. When calculating the latter, we used the (ρ_l, ρ_g, T) data [1], Eq. (11), and the D values determined at the second stage.

Table 2. Densities ($\rho_{mid\,l}$, $\rho_{mid\,g}$) near the critical C_6F_6 isotherms

T, K	$\rho_{mid\,l}$, kg/m^3	$\rho_{mid\,g}$, kg/m^3
515.98	668.94	435.03
516.28	646.49	456.29
516.57	606.49	494.93

The experimental values of ρ_l and ρ_g noticeably deviate from the corresponding calculated values (Table 1). The revealed deviations of the experimental values of the densities show that the (ur_{exp}, h_{texp}, T) data are nonmonotonic. The calculated (h_t, T) data monotonously decrease with increasing temperature (Table 1). Figure 2 shows qualitatively the lines *1*, *2*, and *6,* which correspond to displacements h_t at temperatures 515.98, 516.28, and 516.57 K.

The calculated (ur, h_t, T) data substantially depend on the leading components $Bs_0\tau^\beta$, $Bd_0\tau^{2\beta}$ in accordance with Eq. (11). When approaching T_c, the values of ur and h_t are positive and tend to zero.

The data on h_t, T (Table 1) were used to estimate the average integral density $\rho_{mid\,l}$ in volume V_l from the distribution of $\rho(h - h_m)$ along the isotherms (Fig. 2). For this, it is accepted that the meniscus height h_{mV} = 19.1 mm corresponds to the following boundary conditions:

• the corresponding temperature of the sample is T = 516.57 K (the maximum temperature in the experiment [1]);

• the corresponding displacement of the meniscus is h_{t1} = 0.083 mm (Table 1); this state corresponds to the argument ($h_i - h_m = 0$, $i = 1$) and line *6* (Fig. 2).

At the second stage, the distributions $\rho(h_{ti})$ were obtained at temperatures of 515.98, 516.28, and 516.57 K from the distribution of $\rho(h_i - h_m)$ (e.g., line *5*, T = 516.57 K, Fig. 2).

Hypothesis A, which explains the effect of gravity (g = 9.8 m s^{-2}) on the distribution of $\rho(h_t)$ at a given temperature is considered in the third stage. Within the framework of hypothesis A, several conditions are created in the sample: first, the temperature of the sample corresponds to 516.57 K; its density is $\rho_{cell} \approx \rho_c$ = const; and the meniscus has a shift of h_{t1} = 0.083 mm, which is implemented above under microgravity conditions ($g = g_M$).

Second, the gravity in the cell increases, resulting in a change in the initial distribution ρ(h) that corresponds to microgravity ($g = g_M$) and has a jump of ($\rho_l - \rho_g$). According to hypothesis A, the pressure gradient that arises along the height of the cell upon gravity (g = 9.8 m/s^2) causes a process redistributing molecules in the volume V_l. Therefore, the number of molecules in the elementary volume, which is located below, near the plane S_v with an offset of h_{t1} = 0.083 mm, decreases. The initial density ρ_l, which corresponds to microgravity ($g = g_M$), decreases to the final value $\rho(h_{t1})$ (Fig. 2) at g = 9.8 m/s^2; i.e., the effect $\Delta\rho(T, h) = \rho(h_{t1}) - \rho_l$ caused by gravity (g = 9.8 m/s^2) is negative.

The redistribution of molecules in the elementary volume, which is located near the lower generatrix of the cylinder, significantly changes the initial density ρ_l: it increases to the value of $\rho(h_t)$ since the effect $\Delta\rho(T, h)$ is positive for $h - h_m = 0$.

The initial density profile thus turns into a continuous dependence $\rho(h)$ (Fig. 2, line *5*). According to hypothesis A, the average density $\rho_{mid\,l}$ in volume V_l does not change due to the indicated processes, and the condition of $\rho_{mid\,l} = \rho_l$ is fulfilled.

Based on hypothesis A, we found

(a) the elementary masses $\Delta h_{ti}\, Ls(h_{ti})\rho(h_{ti})$, i = 1, ..., N, where $\Delta h_{ti} = (h_t(i + 1) - h_{ti})$ is the height of the elementary volume, $s(h_{ti})$ is the length of the secant, which refers to the cell section and is separated by h_{ti} from the axis of the cylinder, and N is the number of sections in the interval from 19.1 mm to h_{t1}; and

(b) the elementary volumes $\Delta h_{ti}L_s(h_{ti})$, i = 1, ..., N in the range from h_{t1} to h_{tN}.

At the fourth stage, we performed a numerical integration of the specified masses and volumes in the interval from h_{t1} to h_{tN}. This treatment resulted in the determination of $M_{mid\,l}$, $V_{mid\,l}$ and their ratio, $\rho_{mid\,l}$ = 606.49 kg/m^3 (Fig. 2, line *9*; Table 2), which represents the density of the sample in volume V_l.

$M_{mid\,g}$, $V_{mid\,g}$, and their ratio, $\rho_{mid\,g}$ = 456.29 kg/m^3 (Table 2), which represents the average density of the sample in volume V_g, were calculated similarly.

Figure 3 shows an example of the experimental distribution of $\rho(h)$ (lines *1–3*) from the lower generatrix of the cylinder to the upper one at T = 516.28 K.

At the fifth stage, we determined $\rho_{mid\,l}$ and $\rho_{mid\,g}$ along the isotherms at 515.98 and 516.28 K from the distributions $\rho(h - h_m)$ obtained in experiment II with the calculation circuit considered above (Table 2).

These results made it possible to form a modified array of (ρ_l, ρ_g, T) data, including

• the experimental (ρ_l, ρ_g, T) data [1] at temperatures 298.79–516.57 K, from which points related to temperatures of 515.98, 516.28, 516.57 K are excluded;

• the (ρ_l, ρ_g, T) data contained in Table 2.

Based on the modified data array and NRMS procedure, we calculated the parameters C and D included in models (12) and (13) (Table 3).

The densities ρ_i and local deviations $\delta\rho = 100\ (\rho_i - \rho_{(14)i}/\rho_i$ are calculated, where $\rho_{(14)i}$ is the density value calculated with Eqs. (14) and ρ_i is the density included in the modified (ρ_l, ρ_g, T) data.

Table 3. Parameters of models (12), (13) for C_6F_6

ρ_c, kg/m^3	T_c, K	α,	β	B_{s0}	B_{s1}	B_{s2}
550.77	516.65	0.12985	0.34799	2.14345	0.134753	−1.253085
B_{s3}	B_{s4}	B_{d0}	$B_{d\exp}$	B_{d2}	B_{d3}	B_{d4}
1.40842	−0.897481	0.59485	0.09995	0.042626	1.490123	−2.520365

Thus, Eqs. (14) represent the experimental (ρ_l, ρ_g, T) data [1] with acceptable accuracy in the range of $2 \times 10^{-4} < \tau < 0.2$. The standard deviation for (ρ_l, ρ_g, T) data [1] from the values obtained by Eqs. (14) is defined as $S_g = 0.48\%$ and $S_l = 0.12\%$.

The location of the meniscus under the boundary conditions of experiment I is of interest, because

- ρ_{cell} follows the inequality $\rho_{cell} > \rho_c$ (Fig. 1a, line *3*);
- the temperature T corresponds to the inequality $T < T_{CX}$, where T_{CX} is the temperature that refers to the point c (Fig. 1a) at the saturation curve; the density at point c corresponds to the equality $\rho_l = \rho_{cell}$;
- the gravitational effect is significantly decreased in the cell, e.g., due to its placement in the space laboratory (microgravity conditions, $g = g_M$).

Let us consider state III for a sample in a cell when its parameters correspond to the equalities $T = T_{cross}$, $\rho = \rho_{cell}$ (Fig. 1a, point d); the meniscus displacement $h_t = 0$; the upper and lower parts have a volume of $V/2$.The densities of the substance correspond to the equalities $\rho_g = \rho_g(T_{cross})$, $\rho_l = \rho_l(T_{cross})$.

We transfer the sample to state IV. Its parameters are as follows: $T_{CX} > T > T_{cross}$, $\rho = \rho_{cell}$ (Fig. 1a, point e). In state IV, the meniscus corresponds to line *8* (Fig. 1b). For this state, the mass balance is used, and V_g/V is written as

$$V_g\rho_g + (V - V_g)\rho_l = V\rho_{cell}, \quad \frac{V_g}{V} = \frac{\rho_{cell} - \rho_l}{\rho_g - \rho_l}. \qquad (15)$$

Introducing the functions $\Delta\rho_l$, $\Delta\rho_g$, and $\Delta\rho_{cell} = \frac{\rho_{cell} - \rho_c}{\rho_c}$ in Eq. (15), we can express V_g/V in the form of

$$\frac{V_g}{V} = \frac{\Delta\rho_l}{\Delta\rho_l - \Delta\rho_g} - \frac{\Delta\rho_{cell}}{\Delta\rho_l - \Delta\rho_g}. \qquad (16)$$

We can write the function $\Delta\rho_{cell}$ related to state IV as

$$\Delta\rho_{cell} = \frac{1}{2}(\Delta\rho_l(T_{cross}) + \Delta\rho_g(T_{cross})) = f_d(T_{cross}). \qquad (17)$$

Introducing the displacement of the meniscus h_t into the ratio V_g/V, using Eqs. (10), (16), and (17), we obtain

$$\frac{\Delta V_g}{V} = \frac{4h_tLd}{\pi d^2 L} = \frac{1}{2} - \frac{f_s + f_d}{2f_s}ur - \frac{f_d(T_{cross})}{2f_s}. \qquad (18)$$

Using Eq. (18), we write $h_t(T)$ as

$$h_t = \frac{\pi d}{8}\left(-ur + \frac{f_d(T_{cross})}{f_s}\right). \qquad (19)$$

Equation (19) shows that the displacement h_t substantially depends not only on the ur complex but also on the sample density ρ_{cell}.

SOME NUMERICAL DATA ON THE DENSITY OF SF_6 AND ASSESSMENT OF THE POSITION OF THE MENISCUS IN EXPERIMENT I

In experiment I, we used a cylindrical cell with $d = (10.606 \pm 0.005)$ mm and an effective volume of $V = 221.7$ mm^3. A series of measurements was carried out in the experiment, including the displacement h_t (Fig. 1b, line *13*) and the temperature of a two-phase sample in a given interval under the condition of $\rho_{cell} > \rho_c$. Garrabos et al. [8] presented the results, including

- a graph of the experimental function $y = h_t/r$ in the temperature range of 308 K to temperatures very close to T_c, while the minimum deviation from T_c is ~1 mK;
- the analytical form for the function $y(\tau)$, namely,

$$y = \frac{\pi}{4}\left(-ur + \frac{0.002}{f_s}\right)(1 + x), \qquad (20)$$

where $0.002 = \Delta\rho_{cell} = \frac{\rho_{cell} - \rho_c}{\rho_c}$, $x = 0.06$ is the correction term associated with the effective cell volume.

The following values are given in [8]: $T_c = 318.707297$ K, $T_{CX} = 318.707270$ K, $317.823 > T_{cross} > 318.123$ K, $\rho_c = (742.0 \pm 1.5)$ kg/m^3. The function $y(\tau)$ is shown in Fig. 4 at relative temperatures of $\tau = 10^{-6}$–10^{-2}.

An interesting problem is the construction of (ρ_g, ρ_l, T) data based on the values of (y, T) [8] at relative temperatures $\tau = 10^{-3}$–10^{-6}. At the first stage of the solution of this problem, combined models (12) and (13) were selected to represent the functions f_s, f_d with the values of C and D for SF_6, reported in [3]. In [3], we used the experimental (ρ_g, ρ_l, T) data [9] to calculate the values of C and D at temperatures $\tau = 2 \times 10^{-4}$–0.3. For D values, we presented $T_c = 318.7095$ K, $\rho_c = 741.61$ kg/m^3, $\alpha = 0.1098$, $\beta = 0.34745$, $B_{d0} = 0.25491$, $B_{s0} = 1.9569$, and $B_{d\exp} = 0.08499$.

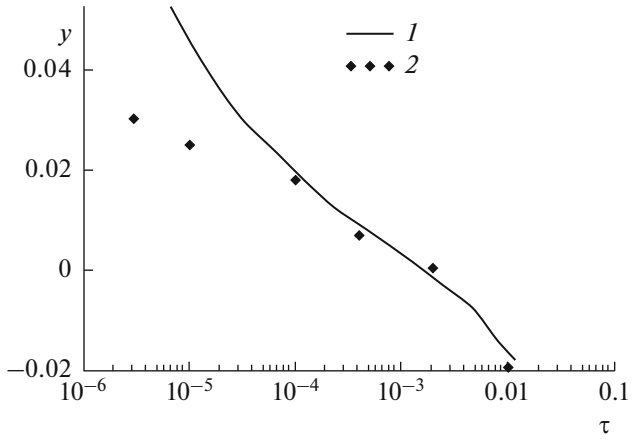

Fig. 4. Dependences of $y(\tau)$: (*1*) $y(\tau)$ (20) and (*2*) experimental (y_{exp}, τ) data.

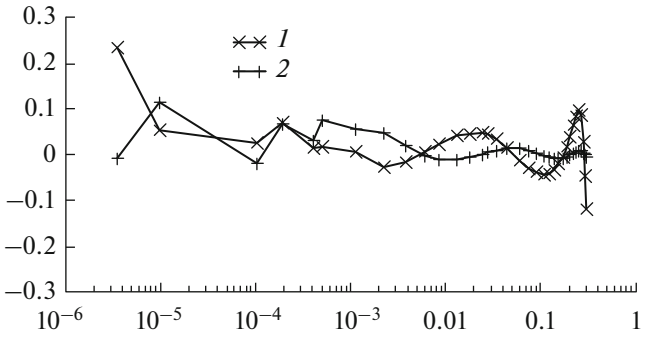

Fig. 5. Comparison of the combined (ρ_l, ρ_g, T) data with the functions $\rho_l(\tau, D, C)$ and $\rho_g(\tau, D, C)$: (1) $\delta\rho_g$ and (*2*) $\delta\rho_l$.

Funke et al. [9] estimated the error $\delta\rho_{exp} \le 0.1\%$ for their (ρ_g, ρ_l, T) data and determined such D values as $T_c = 318.723$ K and $\rho_c = 742.26$ kg/m^3.

Next, the experimental data y_{expi}, T_i, ($i = 1, ..., N$) are selected that were reported in [8] at $\tau = 10^{-3}$–10^{-6} (Fig. 4). Some quantities were calculated based on these values and the function f_s (Eq. (12)), the coefficients of which are given in [3]; some of them are shown in Table 4, i.e.,

• data on f_{si}, T_i ($i = 1, ..., 4$);

• values of ur_i, T_i ($i = 1, ..., 4$) obtained from Eq. (20) and data on y_{expi}, T_i and f_{si}, T_i;

• values of f_{di}, T_i ($i = 1, ..., 4$) obtained from ur_i, T_i and f_{si}, T_i;

• ρ_{gi}, ρ_{li}, T_i ($i = 1, ..., 4$) obtained from Eqs. (14), f_{di}, T_i; f_{si}, T_i, and ρ_c [3].

The combined (ρ_g, ρ_l, T) data was generated. This array combined the data from Table 4 and experimental data [9]. The parameters C, D included in models (12), (13) were determined from this array with the NRMS (Table 5).

Let us compare the results based on the functions $\rho_l(\tau, D, C)$, $\rho_g(\tau, D, C)$ containing the parameters D and C (Table 5). First, the local deviations are calculated $\delta\rho_l = 100(\rho_i - \rho_l(\tau, D, C)/\rho_l$, $\delta\rho_g = 100(\rho_g - \rho_g(\tau, D, C)/\rho_g$. The combined ($\rho_g$, ρ_l, T) data are used for comparison. The standard deviations of the corresponding functions $\rho_l(\tau, D, C)$, $\rho_g(\tau, D, C)$ are defined as $S_g = 0.067\%$ and $S = 0.029\%$. Second, the equations $\rho_l(\tau, D, C)$, $\rho_g(\tau, D, C)$ transmit combined (ρ_g, ρ_l, T) data with an acceptable accuracy in the range of $2 \times 10^{-6} < \tau < 0.3$ (Fig. 5). The (ρ_g, ρ_l, T) data [9] have an error estimated by the authors as $\delta\rho_{exp} \le 0.1\%$.

Third, local deviations of $\delta\rho_l$ and $\delta\rho_g$ (Fig. 6) were obtained, which relate to the (ρ_g, ρ_l, T) array [10]. These experimental results were used in [2–6, 11, 12] to construct the scaling models $f_s(\tau)$, $f_d(\tau)$, $D_m(\tau)$, etc. for SF_6. We estimated the following values:

(a) the arithmetic mean deviation $\delta\rho_{lm} = (\Sigma\delta\rho_{li})/N_2$ ($i = 1, ..., N_2$, $N_2 = 33$) for the (ρ_l, T) data [10] as $\delta\rho_l m = -0.95\%$;

(b) the arithmetic mean deviation $\delta\rho_{gm} = (\Sigma\delta\rho_{gi})/N_2$ ($i = 1, ..., N_2$) for the (ρ_g, T) data [10] as $\delta\rho_g m = -1.05\%$.

Table 4. Some results of the second stage of calculations for SF_6

T, K	y_{exp}	f_s	ur	f_d	ρ_g, kg/m^3	ρ_l, kg/m^3
318.583	0.00712	0.12897	0.00713	0.000923	646.65	837.92
318.678	0.0185	0.07964	0.00351	0.000281	682.76	800.86
318.707	0.0251	0.03576	0.0260	0.000935	715.78	768.81
318.709	0.0315	0.02353	0.0488	0.00115	725.02	759.91

Table 5. Parameters of models (12) and (13) for SF_6

ρ_c, kg/m^3	T_c, K	α_4,	β_4	B_{s0}	B_{s1}	B_{s2}
741.645	318.7101	0.1112	0.3477	1.95825	0.021714	−0.060572
B_{s3}	B_{s4}	B_{d0}	B_{dexp}	B_{d2}	B_{d3}	B_{d4}
−0.938958	1.211974	0.25941	0.08521	1.02283	−0.84764	0.620608

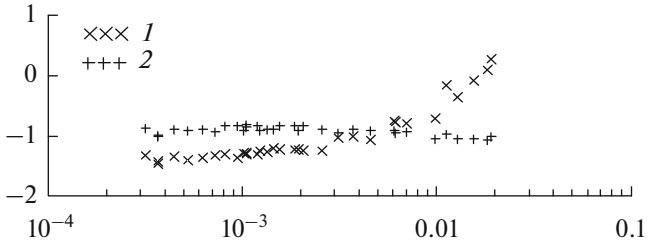

Fig. 6. Comparison of the (ρ_l, ρ_g, T) data from [10] with the functions $\rho_l(\tau, D, C)$ and $\rho_g(\tau, D, C)$: (*1*) $\delta\rho_g$ and (*2*) $\delta\rho_l$.

Several models are studied in the mentioned works, including

(1) the model of the average relative density along the binonodal $f_d = (\rho_l + \rho_g)(2\rho_c)^{-1}$ in the form of $F_d = A_0 + A_1\tau$ [12], where $A_0 = 1.0024$, $A_{1-\alpha} = 1.018$, $T_c = 318.707$ K, and $\rho_c = 733$ kg/m^3;

(2) $F_d = A_0 + A_{1-\alpha}\tau^{1-\alpha}$ [12], where $A_0 = 1.0012$, $A_{1-\alpha} = 0.6909$, and $\alpha = 0.11$;

(3) $f_d = B_{2\beta}\tau^{2\beta}$ [4], where $2\beta = 0.78$, $T_c = 318.707$ K, and $\rho_c = 733$ kg/m^3;

(4) $f_d = B_{1-\alpha}\tau^{1-\alpha} + B_{2\beta}\tau^{2\beta} + B_1\tau + \ldots$ [6] (the results of this model correspond to line *2*, Fig. 1a), where $B_{2\beta} = 1.0864$, $B_{1-\alpha} = -7.990$, $B_1 = 9.770$, $\alpha = 0.11$, $\beta = 0.325$, $T_c = 318.707$ K, and $\rho_c = 733$ kg/m^3.

Models (12)–(14) constructed for SF_6 give an independent basis to estimate the error in the models presented in the literature. As a separate problem, one should consider the issue of a method that makes it possible to the decrease systematic errors of (ρ_g, ρ_l, T) data [10] discussed above. This issue deserves separate consideration.

CONCLUSIONS

We studied the altitude density distribution $\rho(h)$ for a C_6F_6 sample immersed in a cell [1] under gravity ($g = 9.8$ m/s^2). The equation proposed for $h_t(T)$ describes the position of the meniscus in the cell under the boundary conditions $\rho_{cell} = \rho_c$ along the near-critical isotherms under microgravity ($g = g_M$). The resulting equation shows that $h_t(T)$ substantially depends on the complex *ur* and the order parameter f_s.

Some numerical data that relate to temperatures from 515.92 to 516.57 K and include (a) displacements h_t in the range from 0.208 to 0.079 mm and (b) the (ρ_l, ρ_g, T) data were calculated. Based on the combined array of (ρ_l, ρ_g, T) data, we constructed models (12), (13) that are applicable for C_6F_6 in the range of $2 \times 10^{-4} < \tau < 0.2$.

We also proposed an equation for $h_t(T)$ that describes the meniscus position in a cell with a two-phase sample of SF_6 as applied to experiment I under microgravity ($g = g_M$). The selected experimental data included the values $y_i = h_{ti}/r$, T_i ($i = 1, \ldots, N$) [8] in the temperature range of $\tau = 10^{-2}$–10^{-6} and the range of h_t from −0.101 to 0.159 mm. We developed a method that enables

- the calculation of (ρ_l, ρ_g, T) data from the specified (y, T) values;
- the formation of a combined array of (ρ_l, ρ_g, T) data that include new values and points [9] in the range of $2 \times 10^{-6} < \tau < 0.3$;
- the obtaining of parameters D and C of models (12), (13) for SF_6.

The obtained functions $\rho_l(\tau, D, C)$, $\rho_g(\tau, D, C)$ for SF_6 and C_6F_6 satisfactorily describe the corresponding initial (ρ_l, ρ_g, T) data. Thus, the deviation of the combined (ρ_l, ρ_g, T) data, including points [9], is satisfactory ($S_g = 0.067\%$, $S_l = 0.029\%$) in the range of $2 \times 10^{-6} < \tau < 0.3$. The comparison shows that the (ρ_l, ρ_g, T) data [10] contain a systematic deviation of $\delta\rho_m \approx -1.0\%$ in the range of $\tau = 2 \times 10^{-4}$–0.02. The function f_d (Eq. (13)) contains a scaling component ($B_{dexp} > 0$) and does not include a linear term. These features reflect the current trends in the scaling theory [2, 3, 6, 13].

REFERENCES

1. Stankus, S.V. and Khairulin, R.A., *Int. J. Thermophys.*, 2006, vol. 27, no. 4, p. 1110.
2. Vorob'ev, V.S., Rykov, V.A., Ustyuzhanin, E.E., Shishakov, V.V., Popov, P.V., and Rykov, S.V., *J. Phys.: Conf. Ser.*, 2016, vol. 774, 012017.
3. Vorob'ev, V.S., Ochkov, V.F., Rykov, V.A., Rykov, S.V., Ustyuzhanin, E.E., and Pokholchenko, V.A., *J. Phys.: Conf. Ser.*, 2019, vol. 1147, 012016.
4. Losada-Pérez, P. and Cerdeiriña, C.A., *J. Chem. Thermodyn.*, 2017, vol. 109, p. 56.
5. Ustyuzhanin, E.E., Shishakov, V.V., Popov, P.V., Rykov, V.A., and Frenkel', M.L., *Vestn. Mosk. Energ. Inst.*, 2011, no. 6, p. 167.
6. Fisher, M.E. and Orkoulas, G., *Phys. Rev. Lett.*, 2000, vol. 85, p. 696.
7. Anisimov, M.A. et al., *Termodinamika kriticheskogo sostoyaniya individual'nykh veshchestv* (Thermodynamics of the Critical State of Individual Substances), Moscow: Energoizdat, 1990.
8. Garrabos, Y., Lecoutre, C., Marre, S., Beysens, D., and Hahn, I., *Phys. Rev. E*, 2018, vol. 97, 020101.
9. Funke, M., Kleinrahm, R., and Wagner, W., *J. Chem. Thermodyn.*, 2001, vol. 34, p. 735.
10. Weiner, J., Langley, K.H., and Ford, N.C., Jr., *Phys. Rev. Lett.*, 1974, vol. 32, p. 879.
11. Anisimov, M.A. and Wang, J., *Phys. Rev. E: Stat., Nonlinear, Soft Matter Phys.*, 2007, vol. 75, 051107.
12. Pestak, M.W., Goldstein, R.E., Chan, M.H.W., de Bruyn, J.R., Balzarini, D.A., and Ashcroft, N.W., *Phys. Rev. B: Condens. Matter Mater. Phys.*, 1987, vol. 36, p. 599.
13. Ochkov, V.F., Rykov, V.A., Rykov, S.V., Ustyuzhanin, E.E., and Znamensky, B.E., *J. Phys.: Conf. Ser.*, 2018, vol. 946, 012119.

Translated by O. Zhukova